INSTITUTE OF PHYSICS PUBLISHING PHYSICS IN MEDICINE AND BIOLOGY

Phys. Med. Biol. **47** (2002) 3699–3704 PII: S0031-9155(02)39189-9

A terahertz system using semi-large emitters: noise and performance characteristics

G Zhao, R N Schouten, N van der Valk, W Th Wenckebach and P C M Planken

Department of Applied Physics, Faculty of Applied Sciences, Delft University of Technology, Lorentzweg 1, 2628 CJ Delft, The Netherlands

E-mail: planken@tnw.tudelft.nl

Received 1 March 2002
Published 17 October 2002
Online at stacks.iop.org/PMB/47/3699

Abstract

We have built a relatively simple, highly efficient, terahertz (THz) emission and detection system centred around a 15 fs Ti:sapphire laser. In the system, 200 mW of laser power is focused on a 120 μm diameter spot between two silverpaint electrodes on the surface of a semi-insulating GaAs crystal, kept at a temperature near 300 K, biased with a 50 kHz, $\pm$400 V square wave. Using rapid delay scanning and lock-in detection at 50 kHz, we obtain probe laser quantum-noise limited signals using a standard electro-optic detection scheme with a 1 mm thick (110) oriented ZnTe crystal. The maximum THz-induced differential signal that we observe is $\Delta P/P = 7 \times 10^{-3}$, corresponding to a THz peak amplitude of 95 V cm^{-1}. The THz average power was measured to be about 40 μW, to our knowledge the highest power reported so far generated with Ti:sapphire oscillators as a pump source. The system uses off-the-shelf electronics and requires no microfabrication techniques.

1. Introduction

Terahertz time-domain spectroscopy (THz-TDS) has gained widespread popularity in recent years due to the wide range of applications, both in science and technology (Grischkowsky *et al* 1990, Mittleman *et al* 1996, Harde *et al* 1997, Hunsche *et al* 1998). There is currently a great interest in the potential use of THz-TDS for biomedical imaging, in, for example, the early detection of skin cancer. One great advantage of THz radiation is that it is non-ionizing and extremely weak and thus, in all probability, totally harmless to humans. One of the problems faced by people engaged in THz imaging, however, is that for rapid image acquisition, a good dynamic range and signal-to-noise in the detected THz signals are required. This requires both excellent generation and detection techniques. Therefore, to gauge the performance of a THz generation and detection setup, and to facilitate a comparison between different setups,

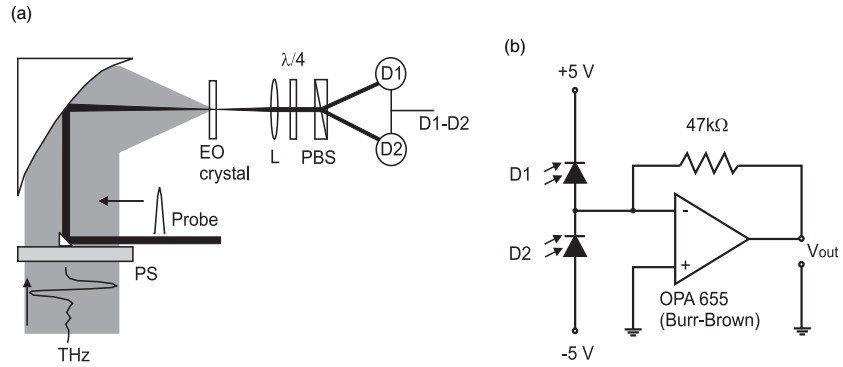

Figure 1. (a) The THz detection setup, with PS a 2 mm thick piece of polystyrene foam, L a lens, PBS a polarizing beamsplitter and $\lambda/4$ a quarter-wave plate. Note the small triangle on the polystyrene plate representing the gold-coated prism. (b) Schematics of the differential detector. D1 and D2 are photodiodes of type BPW34 from Siemens.

a noise analysis is essential. Although such an analysis was given for a THz detection setup based on microfabricated antennas (van Exter and Grischkowsky 1990), a similar analysis is lacking for electro-optic detection.

Here, using an extensive noise analysis, we show that the combination of electro-optic detection and simple, semi-large aperture, biased, semi-insulating GaAs (SI-GaAs) emitters, provides an excellent THz generation/detection system, which can be used for THz spectroscopy and imaging. Surprisingly, we find that biased SI-GaAs with simple, silverpaint electrodes can be a very powerful THz emitter, surpassing the best high power emitters mentioned in the literature for systems using Ti:sapphire oscillators. Using a room-temperature pyroelectric detector for absolute power measurements, we find that approximately 40 μW of THz power can be generated. This number is supported by the value of 95 V cm^{-1} of the THz electric field measured in our electro-optic detection setup. Finally, a comparison with calculations demonstrates that our detection limit is determined by probe laser quantum noise only.

2. Experimental details

The femtosecond laser used in our experiments is from Femtolasers Produktions, Austria. It generates 450 mW of average power, and produces 15 fs pulses with a 72 MHz repetition rate and a centre wavelength of 775 nm. The emitter is a crystal of SI-GaAs (MCP Wafer Technology Ltd), which has a dark resistivity of more than 5×10^7 Ω cm. On the surface of the semiconductor, two crescent-shaped silverpaint electrodes are placed with a smallest separation of 0.4 mm. 200 mW of average laser power is used to illuminate the emitter. A 50 kHz, $\pm$400 V square wave ac bias voltage is applied to the electrodes. A silicon hyperhemispherical lens is glued on the back of the crystal to focus the, initially strongly divergent, emitted radiation in a more forward direction. The optical path of the vertically polarized THz beam is shown in figure 1. After reflecting from several paraboloidal mirrors, the THz beam passes through a 2 mm thick piece of polystyrene foam. The polystyrene foam has a refractive index of 1.017 and an absorption coefficient of less than 1 cm^{-1} for frequencies below 4 THz, and is thus nearly completely transparent in this frequency range, while blocking any remaining near-infrared 'leaking' around the emitter (Zhao *et al* 2002). A small,

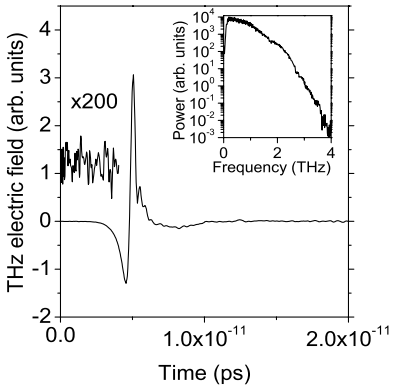

Figure 2. Measured THz electric field as a function of time, obtained using a 1 mm thick (110) oriented ZnTe detection crystal. This measurement corresponds to a total scan time of 20 ms. A signal obtained without the presence of the THz electric field is magnified 200 times and plotted in the same figure. This signal is displaced vertically for clarity. The inset shows the power spectrum calculated from the time-domain signal.

gold-coated, right-angle prism is glued onto the foam. The prism is used to collinearly combine the THz pulse with a synchronized, time-delayed, horizontally polarized probe pulse. Both the THz beam and the probe beam are focused onto the detection crystal, using a 5 cm focal length, gold-coated paraboloidal mirror. The detection process is based on the standard electro-optic detection using a quarter-wave plate, a Wollaston prism and a home-built differential detector. The basic circuitry of this detector is shown in figure 1(b).

3. Results

In figure 2, we plot (top) the THz electric field, measured using a 1 mm thick (110) oriented ZnTe electro-optic crystal (Ingcrys Laser Systems Ltd). This electric-field scan was obtained in a total time of 20 ms. We show the results of a measurement when no THz electric field is present, magnified by a factor of 200, demonstrating the excellent dynamic range of this measurement.

In the inset of figure 2 we plot the power of the THz pulse as a function of frequency. From this figure it can be seen that the spectrum of the THz pulse peaks at roughly 0.5 THz. For this detection crystal, frequency components up to 4 THz are detected. When a 0.1 mm thick (110) oriented GaP crystal is used, components up to 6 THz are detected (not shown here) at the expense of a smaller signal amplitude.

Using 1 mm thick, (110) oriented ZnTe crystal, we measure a relative differential signal $\Delta P/P_{\text{probe}} = 7 \times 10^{-3}$, where $\Delta P = P_1 - P_2$ is the difference in optical power on the two photodiodes, and $P_{\text{probe}} = P_1 + P_2$ is the total probe power. Based on this, we calculate a peak THz electric field of 95 V cm^{-1} (Planken *et al* 2001). With this crystal, we obtain a typical dynamic range of about 5000 for a 35 ps long THz electric-field scan in a time of 20 ms. An independent measurement of the THz power is performed using a room-temperature pyroelectric detector, consisting of a detector element (Eltec), without window or coating, in conjunction with a home-built amplifier. The detector was calibrated using the known power of a helium–neon laser. There is some uncertainty about the response of the detector head at far-infrared wavelengths but it is believed that the response is about 10% lower in the far-infrared. Using this assumption, we deduce an average THz power of

Figure 3. Picture (left) and THz peak-amplitude transmission image (right) of a plastic codekey.

40 μW. To our knowledge, this value, supported by the large value of $\Delta P/P_{\text{probe}}$, represents the strongest THz signal reported in the literature using a Ti:sapphire oscillator as a pump source (Cai *et al* 1997, Wu and Zhang 1997, McLaughlin *et al* 2000, Heyman *et al* 2001, Andrews *et al* 2002).

An example of a THz image obtained with this setup is shown in figure 3. The picture shows the THz peak-amplitude transmission image of a plastic codekey, measured by raster scanning the object through the focus of the THz beam. The THz image (picture on the right) clearly shows the presence (black squares) or absence (white squares) of small magnets contained by the plastic, whereas in the visible region of the spectrum (picture on the left), the plastic is completely opaque. This picture was taken in 8 min, determined by the maximum speed of the *xy*-translation stage. We want to emphasize that, based on the high dynamic range observed in our THz measurements, orders of magnitude faster scanning speeds are, in principle, possible. For example, if it were technically possible to mechanically scan the codekey in 1 s instead of 8 min, the predicted dynamic range per pixel would still be 227, more than sufficient for most applications. The noise properties of the detection setup determine to a large extent whether the signal-to-noise of the setup can be improved or not. The theoretical lower limit of the detector is the shot-noise (sn) limit. With 4.65 mW of average probe power on each photodiode, having a response of 0.49 A W^{-1}, an average current of 2.28 mA is generated. The root-mean-square (rms) shot-noise current fluctuations, expressed in A $Hz^{-1/2}$, can be calculated according to

$$\sqrt{\frac{\overline{(\Delta I_{\text{sn}})^2}}{B}} = \sqrt{2q\,I_0} \tag{1}$$

with q the elementary charge, I_0 the current in the diodes and B the measurement bandwidth in Hz. We find a value of $\sqrt{\frac{\overline{(\Delta I_{\text{sn}})^2}}{B}} = 2.7\times10^{-11}$ A $\text{Hz}^{-1/2}$ for each diode. For the two photodiodes combined, we obtain $\sqrt{\frac{\overline{2(\Delta I_{\text{sn}})^2}}{B}} = 3.82\times10^{-11}$ A $\text{Hz}^{-1/2}$. What is observed in the experiment is the shot-noise voltage V_{sn} generated across the 47 kΩ resistor shown in figure 1(b). We calculate $V_{\text{sn}} = 1.79\times10^{-6}$ V $\text{Hz}^{-1/2}$. We plot this number as the upper horizontal dashed line in figure 4. In the same figure, we also plot the measured noise spectrum of this detector, using a Stanford Research Systems SR760 spectrum analyser, in the range between 1 and 100 kHz. Our THz signals are modulated and detected at 50 kHz and this is therefore the range in which we have to compare the measured and the calculated noise. As seen from the figure, the agreement in this range is excellent, indicating that the detector truly operates in the shot-noise limit. In the same figure, we also plot the measured noise from the differential detector when there is no light on the photodiodes, together with a calculation of the thermal noise generated by the 47 kΩ resistor shown in figure 1. The agreement between the measured and the calculated noise curves shows that without illumination, the noise is

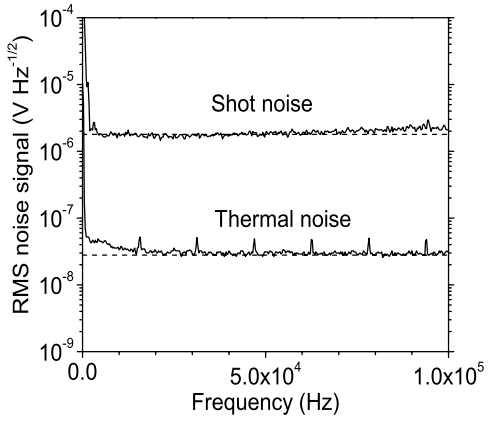

Figure 4. Top curves: measured (solid line) and calculated (dashed line) shot-noise spectra from our differential detector. Bottom curves: measured (solid line) and calculated (dashed line) thermal noise spectra from our differential detector.

mainly determined by thermal noise. The sharp spikes at regular intervals are an artefact caused by magnetic pick-up from the CRT of the spectrum analyser.

We define the noise-equivalent differential power (NEDP) as the minimum detectable probe power difference ΔP_{NEDP}, capable of generating a current equal to the rms shot-noise current. The smallest detectable relative power fluctuations can then also be expressed in terms of

$$\frac{\Delta P_{\mathrm{NEDP}}}{(P_{\mathrm{probe}}\sqrt{B})} = \frac{\sqrt{2\overline{(\Delta I_{\mathrm{sn}})^2}}}{(2I_0\sqrt{B})}. \tag{2}$$

In this equation, the term on the right-hand side constitutes the relative current fluctuations in which the shot-noise $\sqrt{2\overline{(\Delta I_{\mathrm{sn}})^2}}$ is the combined shot-noise of the two photodiodes. Equation (2) is evaluated by using the corresponding currents in the differential detector: an average current of $I_0 = 2.28$ mA runs through each photodiode. This is the current generated by a power $\frac{1}{2}P_{\mathrm{probe}}$. With $\sqrt{\frac{2\overline{(\Delta I_{\mathrm{sn}})^2}}{B}} = 3.82 \times 10^{-11}$ A Hz$^{-1/2}$, we find $\Delta P_{\mathrm{NEDP}}/(P_{\mathrm{probe}}\sqrt{B}) = 8.4 \times 10^{-9}$ Hz$^{-1/2}$. A typical, 40 ps long scan of a THz electric field obtained in 20 ms with a 20 kHz bandwidth, gives $\Delta P_{\mathrm{NEDP}}/(P_{\mathrm{probe}}) = 1.2 \times 10^{-6}$.

Neglecting a small contribution from photodiode dark current, the photodiode shot-noise is the direct consequence of the quantized nature of the probe beam that causes carrier generation. The rms relative fluctuations of the number of photons in the probe beam, as would be measured in a spectrum analyser, using a detector with a 100% quantum efficiency and a bandwidth B, are given by (Haus 2000)

$$\frac{\Delta N_\nu}{N_\nu\sqrt{B}} = \sqrt{\frac{4\pi\hbar c}{P_{\mathrm{probe}}\lambda}} \tag{3}$$

with $\Delta N_\nu = \sqrt{\overline{N_\nu^2}}$ the probe beam photon fluctuations, N_ν the number of photons in the probe beam and λ the wavelength of the probe. We find $\Delta N_\nu/(N_\nu\sqrt{B}) = 7.3 \times 10^{-9}$ Hz$^{-1/2}$. Using the real quantum efficiency of our detector of $\eta = 80\%$, the predicted value for the relative current fluctuations is then $\sqrt{2\overline{(\Delta I_{\mathrm{sn}})^2}}/(2I_0\sqrt{B}) = \Delta N_\nu/(N_\nu\sqrt{\eta B}) = 8.2 \times 10^{-9}$ Hz$^{-1/2}$,

in agreement with the number 8.4×10^{-9} Hz$^{-1/2}$, found earlier. This demonstrates that probe laser quantum noise is the dominant noise source.

Finally, for completeness, we can calculate the lowest detectable THz power in our setup. The maximum peak THz electric field is 95 V cm^{-1}, corresponding to a $\Delta P/P_{\text{probe}} = 7 \times 10^{-3}$. Using the value $\Delta P_{\text{NEDP}}/(P_{\text{probe}}\sqrt{B}) = 8.4 \times 10^{-9}$ Hz$^{-1/2}$ and assuming a reasonable measurement bandwidth of 1 Hz, we obtain $\Delta P_{\text{NEDP}}/P_{\text{probe}} = 8.4 \times 10^{-9}$. We thus have a dynamic range of 8.3×10^5 in electric field, corresponding to a dynamic range of 6.9×10^{11} in THz power. As the THz power associated with 95 V cm^{-1} is 40 μW, the minimum detectable THz power is 5.8×10^{-17} W, a number somewhat better than the number reported by van Exter and Grischkowsky (1990), using microfabricated antennas as THz detectors.

In conclusion, we have described a relatively simple THz generation and detection setup using semi-large aperture emitters and electro-optic detection. Our setup generates up to 40 μW of average THz power with a dynamic range of 6.9×10^{11}, assuming a 1 Hz measurement bandwidth. To our knowledge, this constitutes the highest THz power generated by high repetition rate Ti:sapphire lasers to date. The setup may be ideally suited for biomedical THz imaging experiments which require short data acquisition times.

Acknowledgment

This work was performed as part of the EU TERAVISION programme (IST-1999-10154).

References

Andrews S R, Armitage A, Huggard P G and Hussain A 2002 *Phys. Med. Biol.* **47** 3705–10
Cai Y, Brener I, Lopata J, Wynn J, Pfeiffer L and Federici J 1997 *Appl. Phys. Lett.* **71** 2076
Grischkowsky D, Keiding S, van Exter M and Fattinger Ch 1990 *J. Opt. Soc. Am.* B **7** 2006
Harde H, Cheville R A and Grischkowsky D 1997 *J. Phys. Chem.* A **101** 3646
Haus H A 2000 *Electromagnetic Noise and Quantum Optical Measurements* (Berlin: Springer)
Heyman J N, Neocleous P, Hebert D, Crowell P A, Mller T and Unterrainer K 2001 *Phys. Rev.* B **64** 085202
Hunsche S, Koch M, Brener I and Nuss M C 1998 *Opt. Commun.* **150** 22
McLaughlin R, Corchia A, Johnston M B, Chen Q, Ciesla C M, Arnone D D, Jones G A C, Linfield E H, Davies A G and Pepper M 2000 *Appl. Phys. Lett.* **76** 20
Mittleman D M, Jacobsen R H and Nuss M C 1996 *IEEE J. Sel. Top. Quantum Electron.* **2** 679
Planken P C M, Nienhuys H-K, Bakker H J and Wenckebach W Th 2001 *J. Opt. Soc. Am.* B **18** 313
van Exter M and Grischkowsky D R 1990 *IEEE Trans. Microw. Theory Tech.* **38** 1684
Wu Q and Zhang X-C 1997 *Appl. Phys. Lett.* **70** 1784
Zhao G, ter Mors M, Wenckebach W Th and Planken P C M 2002 *J. Opt. Soc. Am.* B **19** 1476